Available online at www.sciencedirect.com
SCIENCE DIRECT®
Journal of Computational Physics 215 (2006) 1–5
JOURNAL OF COMPUTATIONAL PHYSICS
www.elsevier.com/locate/jcp

Short note

Exact calculation of Fourier series in nonconforming spectral-element methods

Aimé Fournier *

National Center for Atmospheric Research (NCAR), Institute for Mathematics Applied to Geosciences, P.O. Box 3000, Boulder, CO 80307-3000, USA

Received 2 June 2005; received in revised form 30 October 2005; accepted 2 November 2005
Available online 4 January 2006

PACS: 02.30.Nw; 02.60.Cb; 02.60.Jh; 02.70.Dh; 02.70.Jn

Keywords: Adaptive mesh refinement; Fourier analysis; Spectral-element method

1. Usefulness of calculating Fourier series in the SEM

In this note is presented a method, given nodal values on multi-dimensional nonconforming spectral elements, for calculating global Fourier-series coefficients. This method is "exact" in the sense that given the approximation inherent in the spectral-element method (SEM), no *additional* error is introduced that exceeds accumulated computer round-off error. The method would be very useful when the SEM provides an adaptive-mesh simulation of a physical quantity whose global Fourier spectrum is of scientific interest, e.g., in dynamically adaptive fluid-dynamics simulations such as [7].

2. Derivation of an exact transform

Suppose we have some functional problem in a spatial domain $\mathbb{D} := [-\pi, \pi]^d$ (possibly including toroidal geometry) and use coordinate transformations

$$\vec{\vartheta}_k \text{ from } \vec{\xi} \in \mathbb{E}_0 := [-1, 1]^d \text{ to } \vec{x} \in \mathbb{E}_k \tag{1}$$

to partition $\mathbb{D} = \bigcup_{k=1}^{K} \mathbb{E}_k$ by K elements $\mathbb{E}_k := \vec{\vartheta}_k(\mathbb{E}_0)$ with disjoint interiors. Typically, the SEM approximates the exact solution $u(\vec{x})$ by its piecewise degree-p polynomial representation $u^{hp}(\vec{x})$:

$$u(\vec{x}) \approx u^{hp}(\vec{x}) = \sum_{k=1}^{K} \sum_{\vec{\imath} \in \mathbb{I}} u_{\vec{\imath},k} \phi_{\vec{\imath},k}(\vec{x}), \tag{2}$$

* Tel.: +1 303 497 1614; fax: +1 303 497 1646.
E-mail address: fournier@ucar.edu.
URL: http://www.asp.ucar.edu/gtp/fournier.

0021-9991/$ - see front matter
doi:10.1016/j.jcp.2005.11.023

Table 1
Hierarchy of spectral-element Gauss–Lobatto–Legendre (GLL) quadrature nodes and (piecewise) interpolating-polynomial bases

	Nodes	Interpolating basis
1 1D element	$\xi_i \in [-1, 1]$	$\phi_i(\xi) := \sum_{n=0}^{p} \Phi_{i,n} \mathrm{L}_n(\xi)$
1 dD element	$\vec{\xi}_{\vec{\imath}} := \sum_{\alpha=1}^{d} \mathrm{e}^{\alpha} \xi_{\imath^\alpha}$	$\phi_{\vec{\imath}}(\vec{\xi}) := \prod_{\alpha=1}^{d} \phi_{\imath^\alpha}(\xi^\alpha)$
K dD elements	$\vec{x}_{\vec{\imath},k} := \vec{\vartheta}_k(\vec{\xi}_{\vec{\imath}})$	$\phi_{\vec{\imath},k}(\vec{x}) := \begin{cases} \phi_{\vec{\imath}}(\vec{\vartheta}_k^{-1}(\vec{x})), & \vec{x} \in \mathbb{E}_k \\ 0, & \vec{x} \notin \mathbb{E}_k \end{cases}$

The orthonormal Legendre polynomial of degree n on $[-1, 1]$ is $\sqrt{n+\frac{1}{2}}\mathrm{L}_n(\xi)$, w_i is the GLL quadrature weight and $\Phi_{i,n} \equiv w_i \mathrm{L}_n(\xi_i)/\sum_{i'=0}^{p} w_{i'} \mathrm{L}_n(\xi_{i'})^2$ is a Legendre coefficient (e.g. [4, (B.3.15)]).

where "$\approx$" implies the SEM truncation error, h denotes the least $\mathbb{E}_k$ dimension, "$=$" implies machine precision, $\mathbb{I} := \{0, \ldots, p\}^d$ indexes the values $u_{\vec{\imath},k} := u^{hp}(\vec{x}_{\vec{\imath},k})$ and other notation is explained in Table 1. In many scientific applications, such as (magneto-)hydrodynamic turbulence simulation, there are theories to be verified that involve global Fourier-series coefficients $\hat{u}_{\vec{q}}$ at integer wavenumber components q^α. Until now, in usual practice the exact coefficient $\hat{u}_{\vec{q}}$ has been approximated by M^d-point trigonometric d-cubature:

$$u(\vec{x}) \overset{\mathrm{F}}{\leftrightarrow} \hat{u}_{\vec{q}} := (2\pi)^{-d} \int_{\mathbb{D}} u(\vec{x})\, \mathrm{e}^{-\mathrm{i}\vec{q}\cdot\vec{x}}\, \mathrm{d}v(\vec{x}) \tag{3}$$

$$= M^{-d} \sum_{\vec{m}\in\mathbb{M}} u(\vec{x}_{\vec{m}})\, \mathrm{e}^{-\mathrm{i}\vec{q}\cdot\vec{x}_{\vec{m}}} - \mathscr{E}_{\vec{q}} u, \tag{4}$$

where

$$\mathscr{E}_{\vec{q}} u \equiv \sum_{\vec{r}\in\mathbb{Z}^d\setminus\{\vec{0}\}} \hat{u}_{\vec{q}+M\vec{r}} \tag{5}$$

(generalizing [3, Theorem 4.7]), $\mathrm{d}v(\vec{x}) := \prod_{\alpha=1}^{d} \mathrm{d}x^\alpha$ is the volume differential and $\mathbb{M} := \{1, \ldots, M\}^d$ indexes trigonometric nodes $x^\alpha_{\vec{m}} := (2m^\alpha/M - 1)\pi$. Note whenever $\mathbb{D}$ is adaptively repartitioned there is an additional computation cost of at least $\mathcal{O}(\#\{\vec{m}; \vec{x}_{\vec{m}} \in \mathbb{E}_k\})$ per node $\vec{x}_{\vec{\imath},k}$, to use (2) to provide in (4) the values $u^{hp}(\vec{x}_{\vec{m}})$. There is also a d-cubature error $\mathscr{E}_{\vec{q}} u^{hp}$ that by (5) in general converges no faster than $\mathcal{O}(M^{-2})$, because $\mathbb{C}^1$ discontinuities of (2) across element boundaries cause $|\hat{u}^{hp}_{\vec{q}}|$ to decay only as $\mathcal{O}(|\vec{q}|^{-2})$. We discover a more accurate method by substituting Table 1 formulas into (3) to yield

$$u^{hp}(\vec{x}) \overset{\mathrm{F}}{\leftrightarrow} \hat{u}^{hp}_{\vec{q}} \equiv \sum_{k=1}^{K} \sum_{\vec{\imath}\in\mathbb{I}} u_{\vec{\imath},k} \hat{\phi}_{\vec{\imath},k,\vec{q}}, \tag{6}$$

where

$$\hat{\phi}_{\vec{\imath},k,\vec{q}} \equiv (2\pi)^{-d} \int_{\mathbb{E}_k} \mathrm{e}^{-\mathrm{i}\vec{q}\cdot\vec{x}} \phi_{\vec{\imath}}(\vec{\vartheta}_k^{-1}(\vec{x}))\, \mathrm{d}v(\vec{x}) \overset{(1)}{=} (2\pi)^{-d} \int_{\mathbb{E}_0} \mathrm{e}^{-\mathrm{i}\vec{q}\cdot\vec{\vartheta}_k(\vec{\xi})} \phi_{\vec{\imath}}(\vec{\xi}) \left|\partial\vec{\vartheta}_k/\partial\vec{\xi}\right| \mathrm{d}v(\vec{\xi})$$

$$= (2\pi)^{-d} \int_{\mathbb{E}_0} \mathrm{e}^{-\mathrm{i}\vec{q}\cdot\vec{\vartheta}_k(\vec{\xi})} \left(\prod_{\alpha=1}^{d} \sum_{n=0}^{p} \Phi_{\imath^\alpha,n} \mathrm{L}_n(\xi^\alpha) \right) \left|\partial\vec{\vartheta}_k/\partial\vec{\xi}\right| \mathrm{d}v(\vec{\xi}).$$

In many applications, especially when u^{hp}-structure rather than domain geometry guides mesh adaption, each $\mathbb{E}_k$ is a d-parallelepiped with center $\vec{a}_k$ and d legs $2\vec{h}^\alpha_k$, so we have an affinity $\vec{\vartheta}_k(\vec{\xi}) := \vec{a}_k + \vec{\vec{h}}_k \cdot \vec{\xi}$, and so

$$\hat{\phi}_{\vec{\imath},k,\vec{q}} = (2\pi)^{-d} \left|\vec{\vec{h}}_k\right| \mathrm{e}^{-\mathrm{i}\vec{q}\cdot\vec{a}_k} \prod_{\alpha=1}^{d} \sum_{n=0}^{p} \Phi_{\imath^\alpha,n} \int_{-1}^{1} \mathrm{e}^{-\mathrm{i}\vec{q}\cdot\vec{h}^\alpha_k \xi} \mathrm{L}_n(\xi) \mathrm{d}\xi.$$

Finally, recalling the classical identity (e.g. [1, Exercise 12.4.9]) for the spherical Bessel function $j_n(r)$ of the first kind,

$$\mathrm{L}_n(x/\pi) \overset{\mathrm{F}}{\leftrightarrow} \mathrm{i}^{-n} j_n(\pi q), \tag{7}$$

we obtain

$$\hat{\phi}_{\vec{\imath},k,\vec{q}} = \pi^{-d} \left| \overrightarrow{\overrightarrow{h_k}} \right| \mathrm{e}^{-\mathrm{i}\vec{q}\cdot\vec{a}_k} \prod_{\alpha=1}^{d} \sum_{n=0}^{p} \Phi_{i^\alpha,n} \mathrm{i}^{-n} j_n(\vec{q}\cdot\vec{h}_k^{\alpha}). \tag{8}$$

Note that most expressions in (8) can be precomputed; objects that may vary during a dynamically adaptive computation, such as $\vec{a}_k$ or $\vec{h}_k^{\alpha}$, typically take values from a sparse set, e.g., small integer powers of 2. The computation of (6) now incurs no additional error beyond that of (2). Also note, to generalize to the case $p = p_k^{\alpha}$ is straightforward.

3. Accuracy of transform for 1D and 2D test cases

Eqs. (6) and (8) were implemented in MatLab® and tested using known results for (3). The most immediate test is just (7). That (6) verifies (7) can easily be proved to be merely a corollary of the identity

$$\sum_{i=0}^{p} w_i \mathrm{L}_n(\xi_i)\mathrm{L}_{n'}(\xi_i) \equiv \delta_{n,n'} \sum_{i=0}^{p} w_i \mathrm{L}_n(\xi_i)^2 \tag{9}$$

(e.g. [4, (B.2.18)]), so (6) should not perform better on (7) than MatLab® "`legendre`" does on (9), which improves from 11 to 16 digits as p decreases from 18 to 1. This accuracy was verified for (6) applied to (7) for $K = 1$, which implies similar performance on any polynomial $u(\vec{x})$ in this p-range. The next test was to

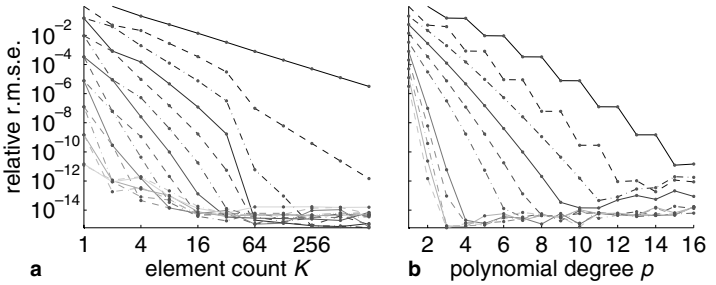

Fig. 1. Relative r.m.s. error in (3) for $u(x) = \sin x$, (a) vs. $K = 2\pi/h$ for $p \in \{1,\ldots,16\}$ (dark to light), and (b) vs. p for $\log_2 K \in \{0,\ldots,10\}$ (dark to light).

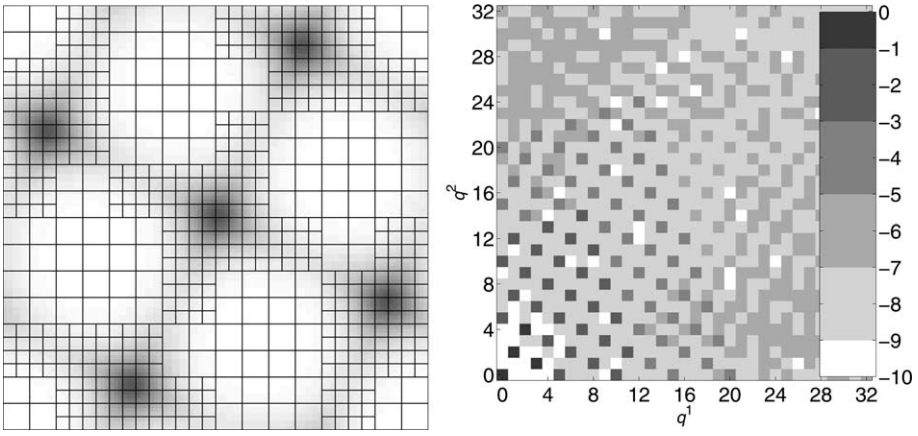

Fig. 2. (Left) u^{hp} (10) over the spatial $\vec{x}$ domain, increasing from light to dark; black lines indicate boundaries of $K = 640$ elements that each contain $(p+1)^2 = 36$ GLL nodes $\vec{x}_{\vec{\imath},k}$. (Right) pixel image of $\log_{10}(|\hat{u}^{hp}_{\vec{q}}|/\max|\hat{u}^{hp}|)$ from (6) vs. q^1 and q^2.

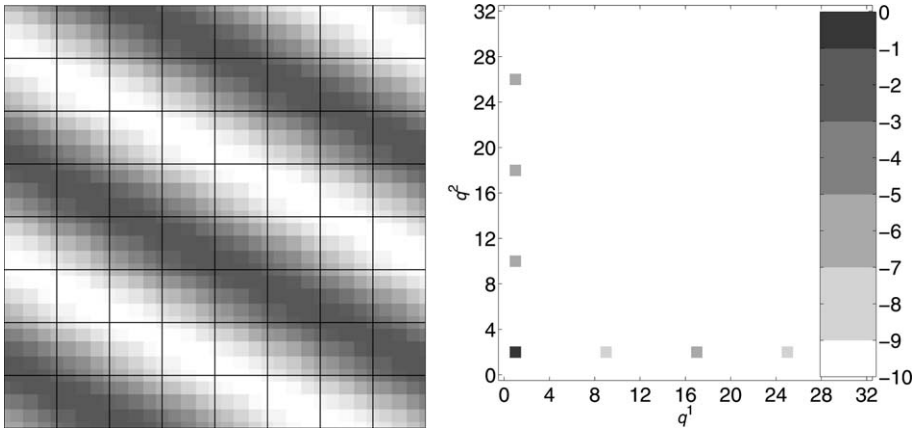

Fig. 3. As in Fig. 2 but for a component of the $t = 0$ state given by (11), in $K = 2^6$ elements.

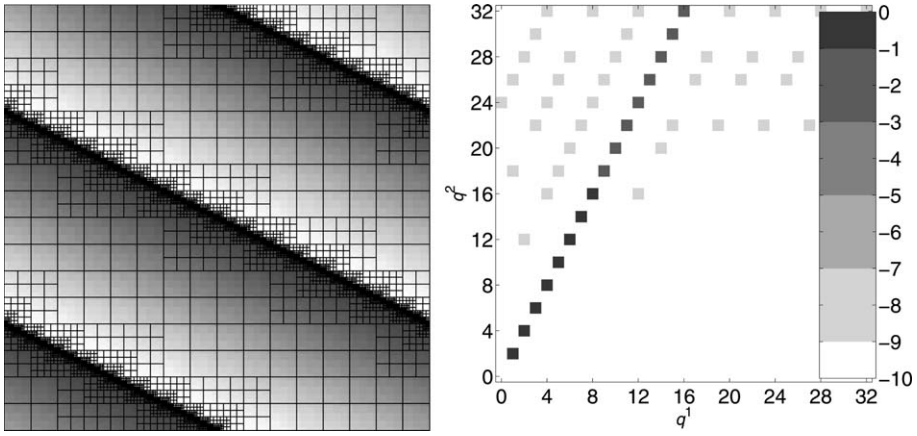

Fig. 4. As in Fig. 3 but for $t = 1.6037/5\pi$ and $K = 18304$ elements.

put $u(x) = \sin x$. Since this is not a polynomial we expect at best to see algebraic convergence w.r.t. K in a uniform meshing $a_k = (k-1)h - \pi$, $h = 2\pi/K$ and exponential convergence w.r.t. p, as verified in Fig. 1. Note there is no need to test $u(x) = \sin rx$ for $r > 1$ because of scaling.

We conclude by examining three 2D tests with adaptive meshing in the fashion of [5], using MatLab®. Fig. 2 shows that (6) verifies (3) in the case [6, (19)]

$$u(\vec{x}) = \sum_{\vec{q}\in\mathbb{Z}^2} \mathrm{e}^{\mathrm{i}\vec{q}\cdot\overrightarrow{\vec{r}}\cdot\vec{x}} \prod_{\alpha=1}^{d} \mathrm{e}^{b^\alpha|q^\alpha|} \equiv \prod_{\alpha=1}^{d} \frac{\sinh b^\alpha}{\cosh b^\alpha - \cos \vec{r}^\alpha \cdot \vec{x}}, \tag{10}$$

where

$$b^\alpha = -\frac{2}{5} \text{ and } \overrightarrow{\vec{r}} \doteq \begin{pmatrix} r^1 & r^2 \\ -r^2 & r^1 \end{pmatrix} = \begin{pmatrix} 1 & 2 \\ -2 & 1 \end{pmatrix}.$$

As might be expected, the $|\hat{u}^{hp}_{\vec{q}}|$ peaks found along $\vec{q}\|\vec{r}$ are found to decay as $|\hat{u}^{hp}_{\vec{q}}| \propto \mathrm{e}^{-0.41|\vec{q}|}$ with a 0.3% residual.[1] In Fig. 3 is shown [6, (22)]

[1] Note, in this plot and those below the $\overrightarrow{\vec{r}}$-operation serves to instigate mesh adaption, but has the consequence of leaving $\vec{q}$ apparently oversampled in $\mathbb{Z}^2$.

$$\vec{u}(0,\vec{x}) := -\vec{r}\sin\vec{r}\cdot\vec{x}. \tag{11}$$

As expected, $\hat{u}^{hp}_{\vec{q}}$ almost vanishes for $\vec{q} \neq \pm\vec{r}$; the six visible coefficients besides $\hat{u}^{hp}_{\vec{r}}$ are all $< 10^{-5}|\hat{u}^{hp}_{\vec{r}}|$, and all other coefficients are $< 10^{-12}|\hat{u}^{hp}_{\vec{r}}|$. Finally, the Burgers equation analytic solution (generalizing [2, (2.5)] to 2D) evolving from (11) at time $t = 0$ to $t = 1.6037/\pi|\vec{r}|^2$ is shown in Fig. 4. As expected for the *nearly* $\mathbb{C}^0$-discontinuous fronts $\perp \vec{r}$ seen at left, $|\hat{u}^{hp1}_{\vec{q}}|$ decays slightly faster than $\mathcal{O}(|\vec{q}|^{-1})$ but *only for wavevectors* $\vec{q}\|\vec{r}$. That is, only 16 coefficients are $> 10^{-7}|\hat{u}^{hp}_{\vec{r}}|$, and they all lie along $\vec{q}\|\vec{r}$ and decay as $|\vec{q}|^{-1.06}$ with a 0.4% residual. Evidently, (8) imparts enough accuracy to (6) to enable very accurate global spectral analysis of characteristic features, even for extremely complex nonconforming element distributions as in Fig. 4.

Acknowledgements

NCAR is operated by the University Corporation for Atmospheric Research and sponsored by the National Science Foundation. The author was also supported by the Office of Science (BER), U.S. Department of Energy, Grant No. DEFG0201ER63247 to the University of Maryland. Any opinions, findings and conclusions or recommendations are those of the author and do not necessarily reflect the views of NSF or DoE.

References

[1] G. Arfken, Mathematical Methods for Physicists, third ed., Academic Press, New York, 1985, 985 pp.
[2] C. Basdevant, M. Deville, P. Haldenwang, J.M. Lacroix, J. Ouazzani, R. Peyret, P. Orlandi, Spectral and finite difference solutions of the Burgers equation, Comput. Fluids 14 (1986) 23–41.
[3] J.P. Boyd, Chebyshev and Fourier Spectral Methods, Springer, Berlin, 1989, 793 pp.
[4] M.O. Deville, P.F. Fischer, E.H. Mund, High-order Methods for Incompressible Fluid Flow, Cambridge University Press, Cambridge, 2002, 499 pp.
[5] A. Fournier, Continuous multiresolution analysis on nonconforming spectral elements, in preparation.
[6] A. Fournier, G. Beylkin, V. Cheruvu, Multiresolution adaptive space refinement in geophysical fluid dynamics simulation, Lecture Notes Comput. Sci. Eng. 41 (2005) 161–170.
[7] D. Rosenberg, A. Fournier, P.F. Fischer, A. Pouquet, Geophysical–astrophysical spectral-element adaptive refinement (GASpAR): Object-oriented *h*-adaptive fluid dynamics simulation, J. Comput. Phys., in press.